Tuning photoenolization-driven cycloadditions using theory and spectroscopy

Jiao Yu J. Wang, Mitchell T. Blyth, Michael S. Sherburn* and Michelle L. Coote*

Research School of Chemistry, Australian National University, Canberra, Australian Capital Territory 2601, Australia

*Email: michael.sherburn@anu.edu.au and michelle.coote@anu.edu.au

ABSTRACT: The first broad spectrum investigation into the photoenolization/Diels-Alder (PEDA) sequence was carried out using M06-2X/6-31+G(d,p) in conjunction with SMD solvation and supported by experimental UV-vis spectroscopy. A test set of 20 pro-dienes was chosen to examine the role of the H atom acceptor group (substituted and unsubstituted carbonyl, thiocarbonyl and imine), the H atom donor group, and bystander ring substituents. As reaction partners for the photogenerated dienes, a diverse test set of 20 dienophiles was examined, comprising electron rich, electron poor, neutral, strain activated, hydrocarbon and heteroatom-containing molecules including CO_2 and CO. A key finding of this work is the demonstration that the PEDA sequence of carbonyl based pro-dienes is tolerant of most substitution patterns. Another is that thiocarbonyl derivatives should behave analogously to the carbonyls but are likely to do so much more slowly, due to an inefficient intersystem crossing, an endothermic 1,5-hydrogen atom transfer (HAT) step and a [1,5] sigmatropic H shift to re-generate the starting material that outcompetes the [4+2]cycloaddition. In contrast, the T_1 state of the *ortho*-alkyl imines displays the incorrect orbital symmetry for 1,5-HAT and is correspondingly accompanied by higher barriers, even in the excited state. However, provided these barriers can be overcome, the remaining steps in the PEDA sequence are predicted to be facile. The Diels-Alder reaction is predicted to be of much broader scope than reported synthetic literature: while electron poor dienophiles are expected to be the most reactive partners, ethylene and electron rich alkenes should react at a synthetically useful rate. CO is predicted to undergo a facile (4+1)cheletropic addition instead of the normal [4+2]cycloaddition pathway. This unique photoenolization/cheletropic addition sequence could provide metal-free access to benzannelated cyclopentanones.

INTRODUCTION

Keto-enol tautomerization is a fundamental process that underpins organic reactivity.[1] Most thermal processes require acid or base catalysis, and proceed via a stepwise mechanism involving successive deprotonation and protonation (or vice versa).[2, 3] However, keto-enol tautomerization can also be triggered photochemically, where it has been harnessed in diverse areas such as natural product synthesis and polymer synthesis.[4] An important class of photoenolization reactions are those of benzaldehydes and acetophenones that carry an *ortho*-CH bond such as **A** (Scheme 1). Orthoquinone dimethides (*o*-QDMs, e.g. **C**) generated in this way have been widely used in [4+2]cycloadditions with dienophiles (**D**) to form cycloadducts **E**.[5, 6]

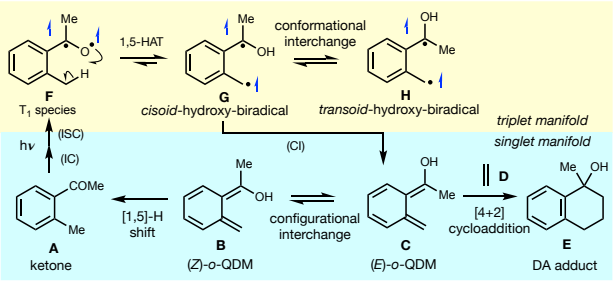

Scheme 1. The prototypical photoenolization/Diels-Alder (PEDA) sequence. Key: IC = internal conversion; ISC = intersystem crossing; HAT = hydrogen atom transfer; CI = conical intersection.

The photoenolization mechanism has been studied spectroscopically and computationally.[4] Photoenolization has been experimentally shown to occur on the triplet surface (Scheme 1, yellow shading).[7-9] The T_1 triplet species **F** readily undergoes 1,5-hydrogen atom transfer (HAT) to generate a relatively stable triplet *ortho*-benzylic biradical **G**. This facile 1,5-HAT must initially form the *cisoid*-hydroxy-biradical **G**, which can isomerize to *transoid*-form **H** through bond rotation. Alternatively, **G** can be converted directly into singlet (*E*)-configured *o*-QDM **C** via a transition state that is close to the conical intersection.[10-12] (*E*)-*o*-QDM **C** can either isomerize to the (*Z*)-*o*-QDM **B** which swiftly tautomerizes back to the starting material **A**, or can undergo the aforementioned Diels-Alder reaction.

This photoenolization/Diels-Alder (PEDA) sequence has been exploited in natural product total synthesis by a number of research groups with selected examples depicted in Scheme 2. The first syntheses were reported by Quinkert (estrone[13, 14]), Prabhakar (alpinigenines[15, 16]), Kraus (podophyllotoxin,[17, 18] anthracycline G-2N,[19, 20] 4-deoxyaklavinone,[21] pleurotin[22, 23]), and Nicolaou (hybocarpone,[24] hamigerans[25]). Recently, the Gao group reported the use of a Lewis acid to facilitate the Diels-Alder phase of the process, permitting the first catalytic enantioselective processes. This methodology has been

applied at an early stage in the total syntheses of oncocalyxone B,[26] mycloeptodiscin A, [27, 28] (+)-xestoquinone and (+)-adociaquinones A/B.[29] The robust nature of the PEDA sequence has also permitted application outside of target-based synthesis such as photoligation,[30] photo-removable protecting groups[31] and photo-activated fragrances.[32]

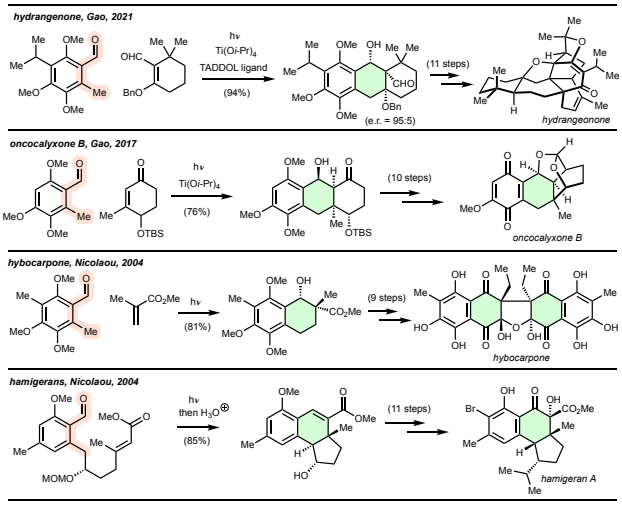

Scheme 2. Selected applications of the photoenolization/Diels-Alder (PEDA) sequence in natural product total synthesis.[24, 26, 33, 34]

To date, most synthetic applications have focussed on the reaction of *ortho*-methyl-benzaldehyde derivatives with C=C dienophiles.[35] With the notable exceptions of trifluoromethyl acetone[36, 37] and CO_2,[38] concerted Diels-Alder reactions with other dienophiles are unexplored. (Stepwise annulations with acylhydrazones[39] and aryl trifluoromethyl ketones[36, 37] have also been described.) Likewise, aside from a series of recent studies of *ortho*-amido imines,[40-43] photoenolization of *ortho*-alkyl imines and thioketones is unexplored (Figure 1). Furthermore, previous computational investigations into this process are limited in scope.[4] In recent findings, steric effects on the (*E*)/(*Z*) isomerization (Scheme 1, **B**/**C**) were identified by comparison of the photoenolization of 4'-*tert*-butyl-2',6'-dimethylacetophenone with 2',4',6'-tri-*iso*-propylacetophenone,[44] while charged substituents on the aromatic ring were shown to alter PEDA reactivity of benzophenone derivatives with CO_2.[12] These studies highlight the potential for manipulating the wavelength of activation and promoting or inhibiting the subsequent reactivity. Herein we report the first broad scope investigation into the influence of structure upon reactivity in the PEDA process (Figure 1).

We identify significant opportunities for expansion in the scope of PEDA processes through insights gained through computational modelling and experimental spectroscopic measurements. Specifically, the influence of four distinct types of aromatic substrate variation upon reactivity are examined (Figure 1). We also examine known PEDA dienophiles and many potentially new ones, through a systematically chosen test set, which examines the importance of electronic activation, strain activation, steric effects and the effect of heteroatom inclusion. Overall, the study aims to redefine the scope and limitations of the PEDA process. We also report a new (4+1)cycloaddition (cheletropic addition) reaction between photogenerated *o*-QDMs **C** (Scheme 1) and carbon monoxide, which could be synthetically valuable for the preparation of indanone systems.

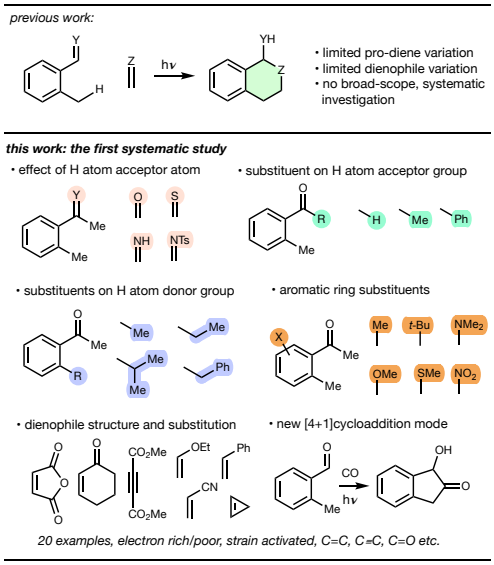

Figure 1. A summary of previous studies into the PEDA sequence and the scope of the current investigation.

RESULTS AND DISCUSSION

To study structure-reactivity trends in PEDA reactions, we conceived a test set of molecules **1**-**20** as precursors to the photogenerated *o*-QDM diene **C** (Chart 1). These structures would identify: (a) the influence of variation in the H atom acceptor heteroatom Y, with carbonyl, thiocarbonyl, imine and *N*-tosylimine groups modeled (**1**-**9**); (b) the effect of substitution at the carbon atom of the H atom acceptor group (**1**-**9**); (c) the influence of substitution upon the H atom donor group (**2**, **10**-**12**); and (d) the effects of substituents of varying steric and electronic demands at different aromatic ring locations (**13**-**20**). First, the PEDA reactions were first screened with three prototypical dienophiles (C_2H_4, CO and CO_2). Next, we computationally examined the PEDA reactions of *ortho*-methyl acetophenone (**2**) with 20 common dienophiles to study strain, steric and electronic effects on the cycloaddition reaction.

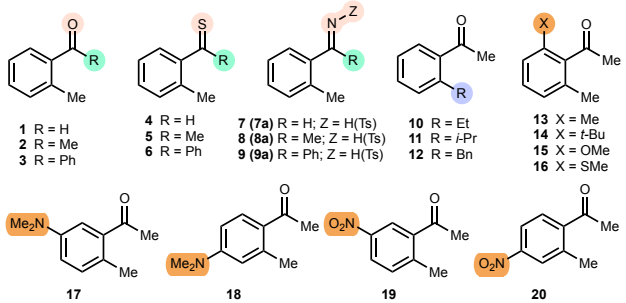

Chart 1. A test set of 20 pro-dienes for PEDA reactions.

During the initial modeling. C_2H_4 and CO_2 were found to react in the expected manner, i.e. as dienophiles in [4+2]-cycloaddition. In the case of CO, however, the (4+1)cheletropic addition was found to be both kinetically and thermodynamically

favored for most of the substrates tested. The photoenolization-cheletropic addition sequence is abbreviated as PECA and is discussed in more detail below (*vide infra*).

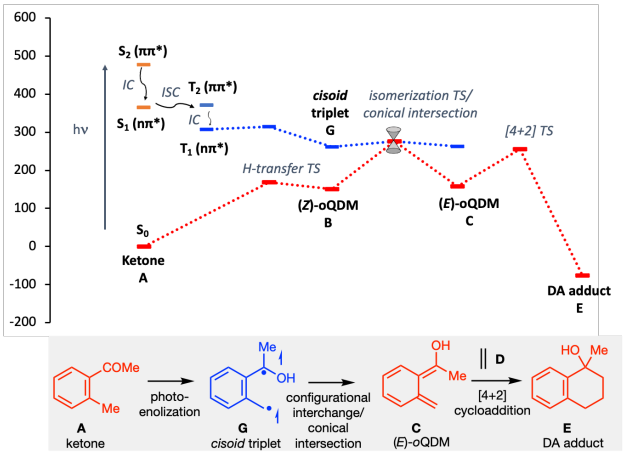

Figure 2. Computed Gibbs free energy surface (kJ mol^{-1} 298 K, DMSO) for the PEDA reaction of *o*-methyl-acetophenone with ethylene. Blue species are triplets and red species are singlets. Calculations performed at the M06-2X/6-31+G(d,p) level with SMD solvent corrections.

Figure 2 shows, as an example, the full potential energy surface for the reaction of the ketone *o*-methyl-acetophenone with ethylene, and serves to summarize what follows; corresponding data for all other systems are provided in the Supporting Information (Appendix S5). We first examine the initial photochemical excitation of the ketone, by computational modelling and experimental UV-vis absorption spectra. We then study the 1,5-HAT process and configurational isomerization steps of the resulting triplet species, the latter of which also corresponds to the conical intersection that returns the molecule to the singlet surface. We conclude by studying the cycloadditions of (*E*)-*o*-QDM with dienophiles.

Photochemistry. To calibrate theory and experiment, a subset of the molecules in Chart 1 – specifically **1**, **2**, **3**, **5**, **6**, **7a**, **8a** and **9a** –were synthesized and their UV-Vis spectra were measured. Attempts to prepare NH imines **7**, **8** and **9** were thwarted by their hydrolytic instability, so the corresponding NTs imines **7a**, **8a** and **9a** were prepared instead. TD-DFT calculations were performed on both NH and NTs imines. Thioaldehyde **4** was likewise unstable and could not be prepared experimentally. TD-DFT calculations were performed on the full test set and complete data is provided in Appendix S4 of the Supporting Information.

Figure 3 shows experimental and computed spectra for *o*-methyl benzophenone **3** and its thiocarbonyl (**6**) and NTs imine (**9a**) derivatives along with their associated Jablonski diagrams; spectra for the other compounds studied are displayed in Appendix S2 of the Supporting Information. Figure 4 shows eight grouped sets of calculated spectra to identify the influence of different structural variations upon absorption maxima. Experimental spectra show good qualitative agreement with calculations performed at the M06-2X/6-31+G(d,p) level. We also benchmarked our computational spectra using CAM-B3LYP and ω-B97XD with the 6-31+G(d,p) and Def2-TZVP basis sets, (see Appendix S4 of the Supporting Information) and found that the level of theory did not significantly affect the observed spectra.

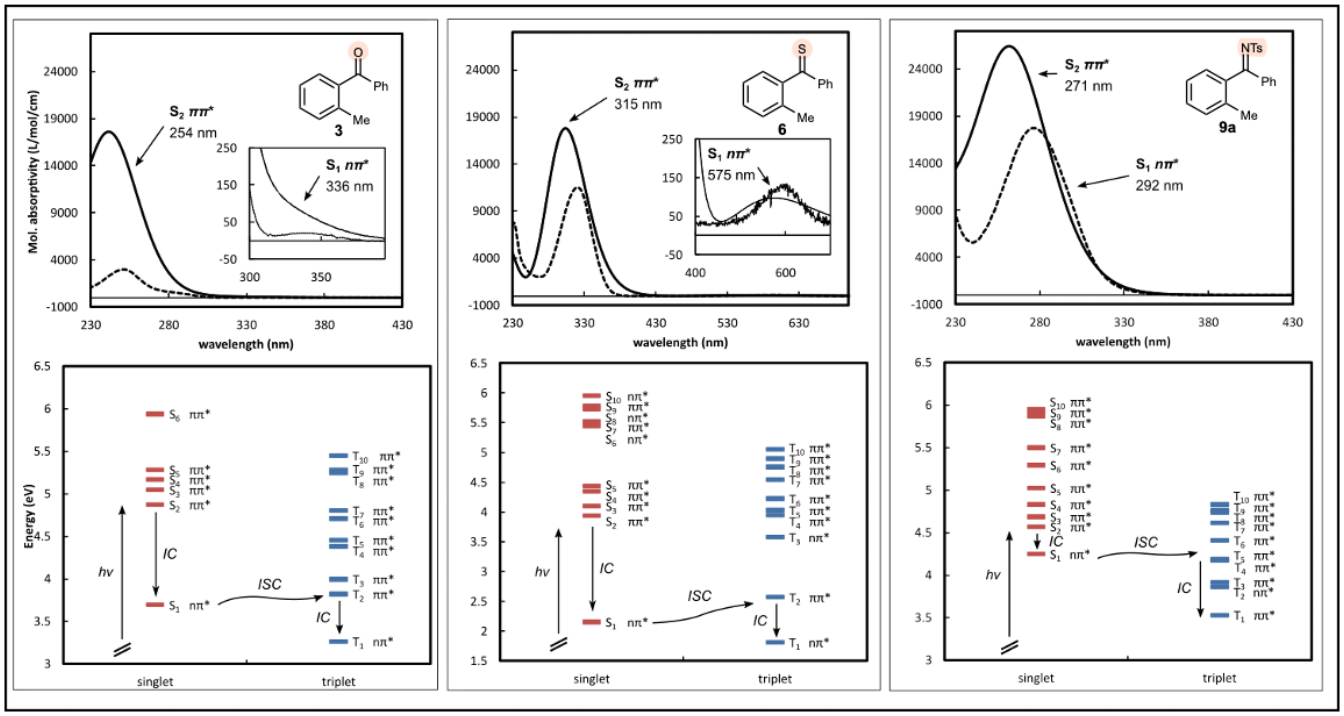

Figure 3. Calculated and measured UV/vis spectra (298 K, DCM) and associated Jablonski diagrams for *ortho*-alkyl acetophenone and its thioketone and NTs imine derivatives. Solid line = calculated spectrum at M06-2X/6-31+G(D,P) level of theory. Dashed line = experimentally

measured spectrum in dichloromethane. Corresponding data for the other compounds are provided in Appendix S2 of the Supporting Information.

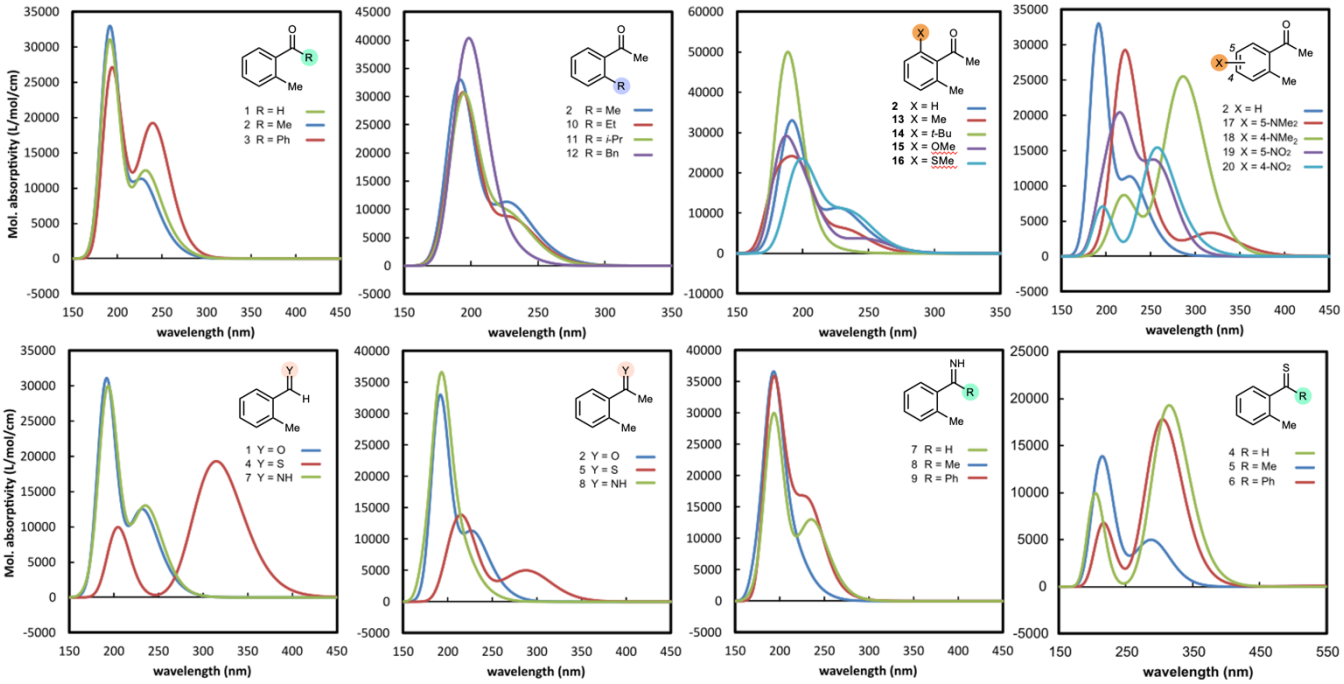

Figure 4. Effect of substituents on the calculated UV/vis spectra (298 K, DMSO) *o*-alkyl acetophenone and thiocarbonyl and imine derivatives. Jablonski diagrams and data in other solvents are provided in Appendix S4 of the Supporting Information.

o-Methyl benzophenone (**3**) shows a strong absorption at around 250 nm, which corresponds to the S_2 ($\pi\pi^*$) transition. Following internal conversion to the S_1 ($n\pi^*$) state, this would be expected, by El Sayed rules,[45] to undergo rapid intersystem crossing to the nearby T_2 ($\pi\pi^*$) state, followed by internal conversion to the reactive T_1 ($n\pi^*$) state. The other ketone derivatives display similar behavior, both with respect to their Jablonski diagrams (Appendix S4) and their UV-Vis spectra (Figure 4). As expected, absorptions are red-shifted when the extent of conjugation is increased, and this is most pronounced when a *p*-NMe_2 ring substituent is included (**18**), as this results in captodative interactions with the carbonyl.

Based on the experimental and computational spectra, one would expect the optimal wavelength for photoenolization of acetophenone and its various substituted derivatives to be around 230-260 nm. However, experimental conditions typically use UVA sources,[24, 26, 33, 34] where the molecule absorbs only weakly. Indeed, action plots for these reactions are typically red-shifted from the absorption spectra, and show significant so-called "dark" reactivity in the near UV region.[11] Although ~250 nm is the brightest (i.e., highest oscillator intensity) state accessible with conventional UV sources, absorption into this would likely result in significant side reactions. The S_1 state (~330 nm in **3**) absorbs weakly but still has a non-negligible oscillator intensity, is more likely to offer a better trade-off between reactivity and selectivity. Consistent with this, a recent study of the PEDA reaction of a derivative of **15** with *N*-ethyl maleimide found optimal yields at this wavelength.[11]

The thiocarbonyl compounds exhibit UV/vis spectra that are similar to the carbonyl series but, as expected for the heavier sulfur atom, the peaks are significantly red-shifted (compare **6** vs. **3**, Figure 3; **4** vs. **1** and **5** vs. **2**, Figure 4). Because the $n\pi^*$ and $\pi\pi^*$ transitions are affected to different extents, the T_2 state ($\pi\pi^*$) now lies significantly above S_1 ($n\pi^*$) and intersystem crossing is expected to be less efficient.

The imines behave differently to the ketones and thioketones in that their lowest triplet state T_1 now has $\pi\pi^*$ character and not the $n\pi^*$ character expected for subsequent PEDA reactivity. In practical terms, this means that, in the T_1 state, the SOMO on the heteroatom of the imines no longer lies in the same plane as the H-atom donor but rather is orthogonal to it (see Appendix S4.7 of the Supporting Information). This does not render HAT impossible but rather the molecule has to undergo greater geometric distortion to react and this is associated with a significantly higher reaction barrier (*vide infra*). As a result, both radiative and non-radiative transitions back to the ground state are likely to be competitive with HAT and this accounts for why there are so few examples of imine-based PEDA reactions in the literature. To the best of our knowledge, the Kutateladze group[40-43] has developed the only synthetic examples of PEDA reactions using imines as H atom acceptors, and all examples specifically involve amide (i.e., N–H bond) H atom donors. Interestingly, prior theoretical and experimental studies suggest that photoenolizations involving N–H[46-49] and O–H hydrogen atom donors[50-53] are different from C–H HAT processes in that they occur from a singlet $\pi\pi^*$ state, rather than a triplet $n\pi^*$ state.[54]

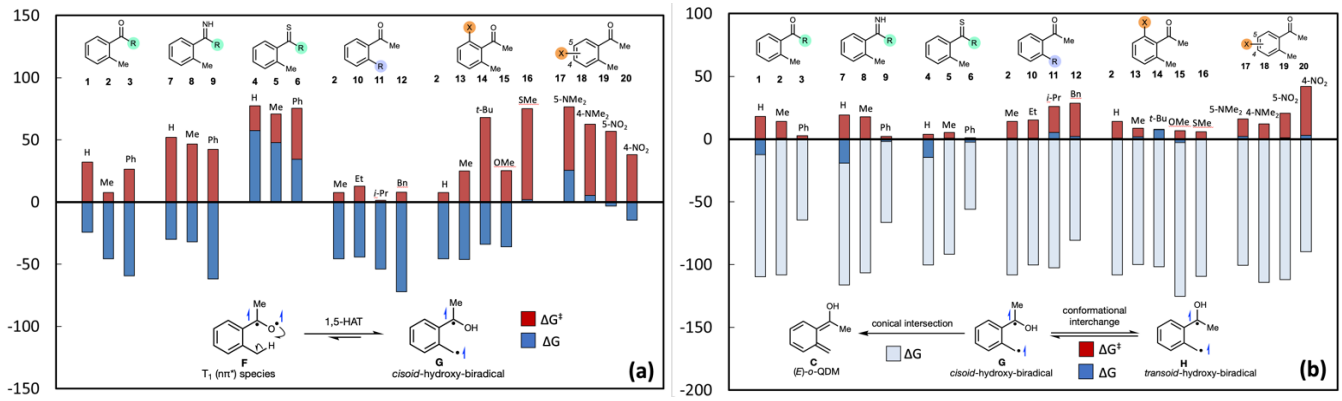

Figure 5. (Gibbs free energy barriers and reaction energies (kJ mol^{-1}, 298 K, DMSO) for (a) the excited state hydrogen atom transfer reaction, and (b) the isomerization reaction on the triplet surface (**G** to **H**), as well as the overall Gibbs free energy between the triplet *cisoid*-hydroxy species (**G**) into the (*E*)-*o*-QDM (**C**).

To generalize PEDA reactions to *o*-alkyl imines, it may be necessary to re-order the excited states. Our recent theoretical and experimental work on acetophenone derivatives used as Type I photo-initiators suggests that this may be possible using the electrostatic effects of charged substituents or Lewis acids due to the different polarities and polarizabilities of the nπ* and ππ* states.[12, 55-58] Work involving *o*-alkyl imines is currently underway.

Hydrogen atom transfer and *cisoid*→*transoid* hydroxy biradical isomerization. Excited-state 1,5-HAT Gibbs free energy barriers and reaction energies were calculated from the triplet T_1 state (see Figure 5a). In general, the favorability of intramolecular hydrogen atom transfer decreases along the series: O > N > S. In the oxygen case (Scheme 1), the ketone-derived T_1 species **F** has a relatively high energy and the formation of the triplet *ortho*-benzylic biradical **G** is energetically favorable. The opposite is observed for the sulfur-containing compounds. In this case, the T_1 thioketone is lower in energy but the pathway to the 1,5-HAT product is endergonic. This is because the 1,5-HAT reaction in the ketone is driven by the conversion of the less stable alkoxy radical into the more stable benzylic radical (Scheme 3). This driving force is absent in the thioketone as the more polarizable thiyl radical is more inherently stable to begin with.[59, 60] The behavior of the imines is intermediate. The nitrogen-centered radicals have a similar thermodynamic driving force for the HAT reaction to the alkoxy radicals but considerably higher reaction barriers as a result of the reactant T_1 state having the incorrect orbital symmetry (*vide supra*).

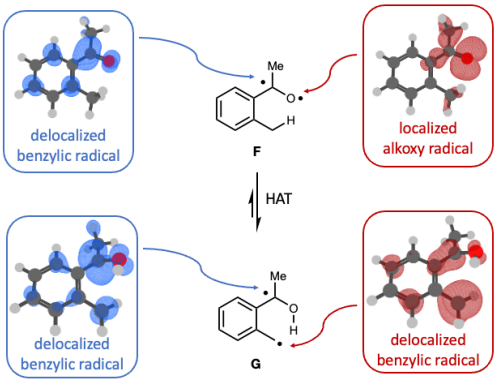

Scheme 3. The singly-occupied molecular orbitals of triplet *o*-alkyl-acetophenone species **F** and 1,5-HAT product **G** calculated at the RO-M06-2X/6-31+G(d,p)//M06-2X/6-31+G(d,p) level of theory; isovalues chosen to make the orbital surface areas consistent.

Within the ketones (**1**-**3**, **10**-**20**), substituent effects on the thermodynamics of the HAT reaction follow expectations based the ability of the substituents to better stabilize the reactant T_1-keto (**F**) or product *cisoid*-enol (**G**). For instance, the stabilizing effect of *gem*-dimethyl (**11**) or phenyl (**12**) substitution at the H atom donor site is significant in the product radical but not the reactant radical and these promote the HAT reaction compared with the corresponding unsubstituted (**2**) and methyl (**12**) substituted compounds. Thermodynamic favorability for the HAT reaction also increases as the ketone R group is changed from **1** (R=H) to **2** (R=Me) to **3** (R=Ph), reflecting the increasing ability of this group to stabilize the adjacent benzylic radical. While these groups stabilize both the reactant and product radical, the latter effect is greater due to additional captodative stabilization of the OH group in the product. Similar arguments around captodative stabilization also explain the effects of 4- and 5-NMe_2 and NO_2 ring substituents (compare **2** with **17**-**20** in Figure 5a). Within the ketones, the kinetics of the HAT reaction largely follow thermodynamics except where stabilizing polar effects (e.g. **2** versus **1** or **3**) or destabilizing steric effects (e.g. **14** versus **15**) participate.

Figure 5b shows the isomerization barriers and reaction Gibbs free energies on the triplet surface, as well as the overall energy change from the triplet *cisoid*-hydroxy species into the (*E*)-*o*-QDM. It is important to note that the isomerization transition state is close to a conical intersection that returns the hydroxy biradical to the singlet surface[10-12]; as such, it functions as a kinetic trap. On the triplet surface, reaction energies are close to zero except when there are differential steric effects or hydrogen bonding in the product and reactant alcohols (or corresponding amines/thiols). The energy change from the triplet *cisoid* hydroxy species to the (*E*)-*o*-QDM is of course highly exergonic in all cases due to the π-bond formation that accompanies it. The barriers also fall into a relatively narrow range, with two notable exceptions. Delocalization of the radical onto R (the substituent on the H atom

acceptor group) is not disrupted by bond rotation and hence when R is phenyl the isomerization barriers are much lower than otherwise (compare $\Delta G^{\ddagger}$ for **3** vs. **2**/**1**, **9** vs. **7**/**8**). The barriers are lower than expected for the thiol derivatives **4**-**6**, presumably due to longer C–S vs. C–O bond lengths, and hence decreased steric clashing in the (*E*)-*o*-QDM. These low barriers for the thiols allow the (*E*)-*o*-QDM form to be kinetically trapped, even though the HAT reaction is itself energetically unfavorable, and indicate that PEDA reactions with these substrates, while more inefficient, may be feasible.

Cycloaddition Patterns of Reactivity. As shown in Scheme 1, after passing through the conical intersection, the (*E*)-*o*-QDM **C** is formed and can undergo a [4+2]cycloaddition with a dienophile **D**. Alternatively, it can isomerize back to the (*Z*)-*o*-QDM **B**, which, since it is now on the singlet surface, will rapidly undergo a [1,5]-sigmatropic H shift back to the starting material **A**. As a result, while the (*E*)- and (*Z*)-*o*-QDMs can both undergo cycloadditions reactions in principle, in practice they are only kinetically competitive from the (*E*)-form (where competing [1,5]-sigmatropic rearrangement is not possible). Even for the (*E*)-*o*-QDM **C**, cycloaddition must outcompete geometrical isomerization, and so both barriers are important in determining the outcome of the process. As an initial screening study, we examined the cycloaddition of every one of our 20 (*E*)-*o*-QDMs with three prototypical molecules: CH_2CH_2, CO_2 and CO (Figure 6). In all cases, CO_2 and ethylene undergo [4+2]cycloadditions to form six membered ring products. For the CO_2 cycloaddition products, the favored lactone regioisomer is the one where the incoming CO_2 dienophile and hydroxy-(*E*)-*o*-QDM diene **C** are polarity matched. Under typical experimental conditions, these hydroxylactone products **I** tautomerize to the more thermodynamically stable *ortho*-acetyl benzoic acid.[12, 38]

For the ketones and thioketones, CO reacts preferentially *via* a cheletropic (4+1)cycloaddition pathway to form benzannelated cyclopentanones **J** (Figure 6A). This is an interesting process, since concerted cheletropic (4+1)cycloadditions involving CO are, to our knowledge, unknown,[61] despite such processes being highly sought after.[62] It is the reverse of this process, specifically the cheletropic *elimination* of CO that is generally encountered synthetically.[63, 64] The selectivity for the (4+1)- instead of the [4+2]cycloaddition is almost certainly driven by the strong thermodynamic preference (of ca. 200 kJ mol^{-1}) to form the indanone **J** instead of the considerably less stable heterocyclic carbene **K**. Notably, for the imine-containing substrates, while there is still a very strong thermodynamic preference for (4+1)cycloaddition over [4+2]cycloaddition, the [4+2] process has a lower barrier. At the same time, because the [4+2] process is so thermodynamically disfavored, it is unlikely to be the final product of the reaction unless substrates were designed to intercept the carbene via a fast intramolecular reaction. In this case, an initially formed [4+2]cycloadduct would most likely form reversibly, ultimately leading to the (4+1)cycloadduct, in a similar manner to that encountered in reactions between *o*-QDMs and SO_2.[65]

Figure 6 shows the (kinetically preferred) barriers and reaction Gibbs free energies for the cycloadditions (in red and blue bars, respectively), with the competing (*E*)/(*Z*) isomerization barrier (black bar) shown for comparison. For *o*-methyl acetophenone **2**, barriers to reaction with CO, CO_2 and ethylene are relatively similar and thermally accessible, and all easily outcompete isomerization. The same is true for *o*-methyl benzaldehyde **1**, but for *o*-methyl benzophenone **3** the (*E*)/(*Z*) isomerization barrier is considerably lower for reasons discussed

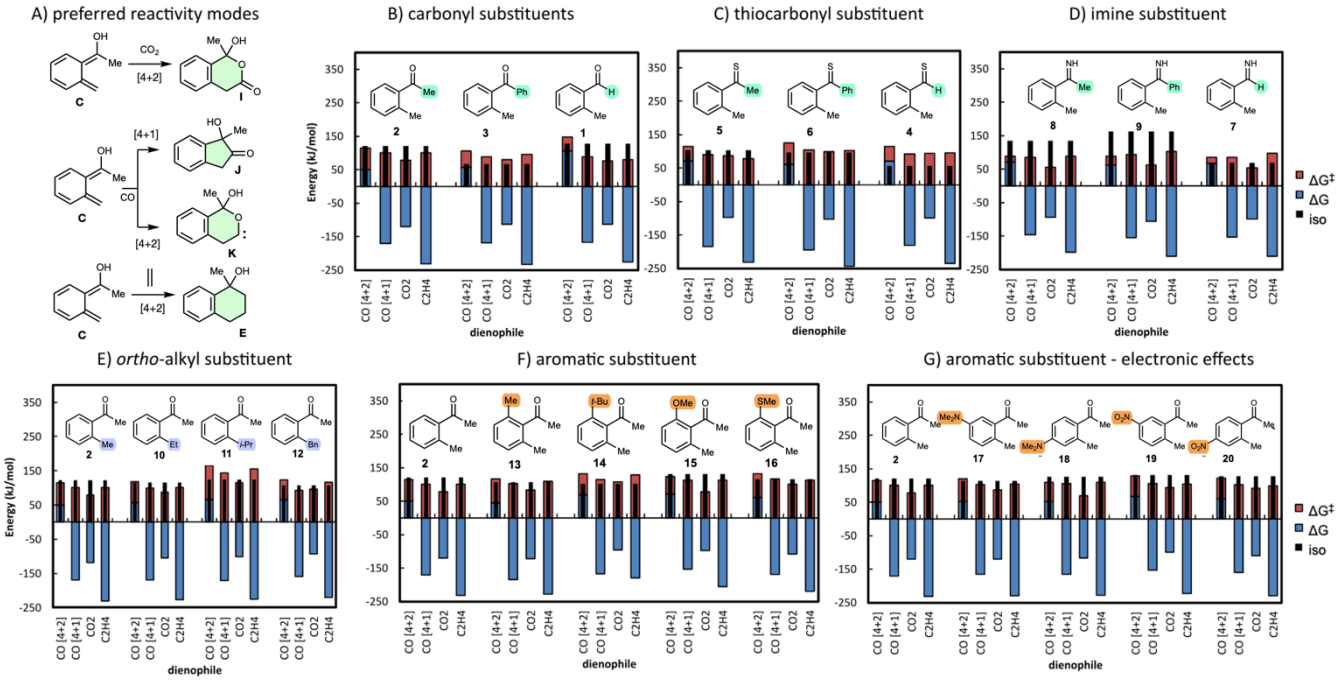

Figure 6. Gibbs free energy barriers (red bar) and reaction energies (blue bar) (kJ mol^{-1}, 298 K, DMSO) for cycloadditions between the *ortho*-alkyl acetophenones and their derivatives with prototypical dienophiles CO, CO_2 and C_2H_4. The competing *E/Z* isomerization barrier is shown for comparison (black bar). All barriers and reaction energies correspond to their preferred modes of reactivity. These are shown in panel A)

using acetophenone as an example; all other substrates show the same regioselectivity except for the reaction of CO with the imines, for which [4+2]cycloaddition is kinetically but not thermodynamically preferred over (4+1) cheletropic addition. Results are shown as a function of B) carbonyl substituents C) thiocarbonyl substituents D) imine substituents E) *ortho*-alkyl substituent F) peripheral *ortho*- substituents G) aromatic electron donating / withdrawing groups.

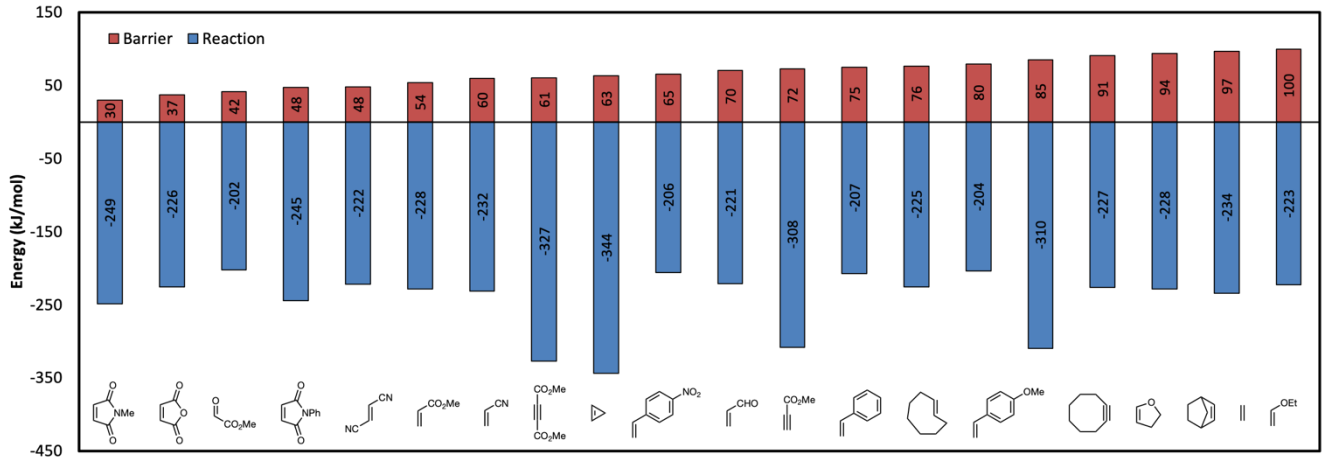

Figure 7. Gibbs free energy barriers (red) and reaction energies (blue) (kJ mol^{-1}, 298 K, DMSO) for the most kinetically favorable Diels-Alder reaction between the (*E*)-o-QDM form (**C**) of *ortho*-methyl acetophenone **2** and the test set of 20 dienophiles, arranged in order of increasing barrier height.

above. As a result, regeneration of the starting material through geometrical isomerization followed by [1,5]-sigmatropic rearrangement will decrease the efficiency of the PEDA process. For the corresponding thioketones and imines, cycloaddition barriers are similar to the ketones, but the isomerization barriers are larger and smaller, respectively. What this means is that, if the inefficiencies of the photochemistry could be overcome, the imines should be suitable reactants for PEDA chemistry, while for the thioketones the substrate scope would be more limited.

Figure 6E shows the effect of the *ortho*-alkyl substituent on the (4+1) and [4+2]cycloaddition. For a given model dienophile, the thermodynamics remain similar, irrespective of the pro-diene's *ortho*-substituent. In terms of barrier, the substrates possess a similar reactivity profile with the exception of isopropyl derivative **15**, which has notably higher barriers as a result of steric effects. Figure 6F shows the effect that a second, *ortho*-substituent has on Diels-Alder / (4+1) reactivity. In general, the presence of the second *ortho*-substituent increases the cycloaddition barrier due to unfavourable steric interactions between the spectator *ortho*-substituent and the C(Me)OH group of the *o*-QDM. A notable exception is **16** in which, as noted previously,[11] the *ortho*-methoxy-substituent undergoes favourable hydrogen bonding with the C(Me)OH group of the *o*-QDM, which makes the diene more electron rich and thus a better electronic match with an electron deficient dienophile such as CO_2.

Figure 6G shows the effect of strong electron donating / withdrawing spectator aromatic substituents. Notably, when an electron withdrawing group is *para*- to the carbonyl (substrate **21**), the (*E*)/(*Z*) isomerization barrier is greatly increased. Presumably this is due to the captodative effect of the hydroxyl- and nitro-groups in the *o*-QDM structure, which stabilizes it through conjugation. Consistent with this conjecture is the fact that an electron donating group at the *para* position (substrate **19**) does not decrease the isomerization barrier relative to the unsubstituted system. Instead, it lowers the CO_2 [4+2]cycloaddition barrier below that of the *ortho*-methoxy substrate **16** – another finding that should have significant synthetic value.

Cycloaddition Structure-Reactivity Trends. Finally, we were interested in understanding the scope of Diels-Alder reactivity from a prototypical *o*-alkylacetophenone **2** against a broad variety of common dienophiles. Our 20 dienophile test set is shown in Figure 7, and covers electron-rich, electron-poor, electronically neutral (unactivated) systems, and strain-activated examples. It includes carbo-dienophiles and heterodienophiles, double and triple bonded systems. As expected,[66] the electron-rich *o*-QDM diene is predicted to be most reactive towards strongly activated dienophiles such as *N*-methyl maleimide, maleic anhydride, and methyl glyoxylate; conversely, reactions with relatively electron-rich dienophiles such as ethoxyethene will be slower due to higher reaction barriers. Importantly, none of these barriers should be prohibitively high to require strong heating or catalysts for cycloaddition. Thus, the boosted reactivity of the *o*-QDM system (relative to a simple 1,3-butadiene that does not generate an aromatic ring on cycloaddition) results in even ethylene reacting at a reasonable rate. Reactions involving alkynes and some of the strain-activated examples display particularly exothermic reactivity. All reactions for which *endo-exo* stereoselectivity are possible were found to be *endo*-selective.[67]

Figure 8 demonstrates the relationship between the transition state asynchronicity,[68] or the absolute difference in bond lengths for the two forming bonds in the Diels-Alder transition state, and the barrier heights for each of the kinetically-preferred reactions involving the dienophiles presented in Figure 7. We find that, in general, activated dienophiles are more

asynchronous and display a positive relationship between asynchronicity and barrier height, whereas electron-rich and strain-activated dienophiles in our test set are less asynchronous and display either a weak inverse relationship between barrier height and asynchronicity (electron-rich), or no clear relationship (strain-activated). Enhanced asynchronicity in Diels-Alder reactions is generally assumed to be accompanied by lower barriers,[69] hence our findings with dienophiles that are electronically well matched to the hydroxy-*o*-QDM are surprising and demand further investigation. Irrespective of these fascinating mechanistic insights, the results from Figures 7 and 8 suggest that the dienophile scope of PEDA sequences is much wider than presently assumed.

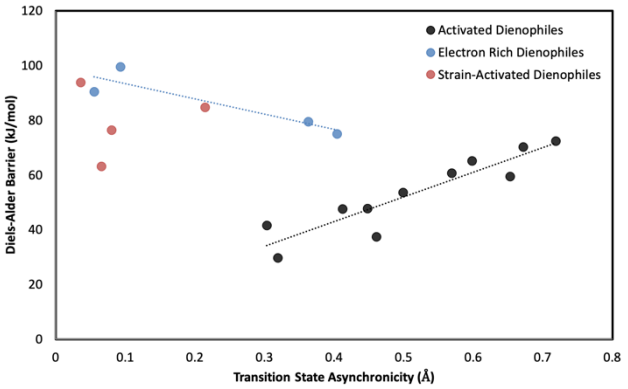

Figure 8. The relationship between transition-state barriers and transition-state asynchronicity (absolute difference in bond lengths for the two forming bonds in the Diels-Alder transition state) for each of the preferred Diels-Alder reactions for each of the dienophiles in our test set. Lines are drawn to guide the eye and are not intended to imply a linear relationship.

CONCLUSIONS

The photoenolization/Diels-Alder (PEDA) sequence between *ortho*-acetophenones and dienophiles is finding increasingly high-profile applications in target molecule synthesis, CO_2 storage and photoligation applications. The process involves the generation of transient *ortho*-quinonedimethide intermediates. Despite its successes, reported examples of the process define a restricted structural space. Herein we used theory supported by spectroscopy to significantly expand the scope of the process, through the first broad spectrum structure-reactivity investigation of the four major productive steps of the PEDA process.

To date, no synthetic applications of *ortho*-alkyl thiocarbonyl and imine derivatives have been reported. This work shows that, in principle, both should be accessible through rational substrate design. These studies should address the problem of enolization, which in the thiocarbonyl series this is hampered by thermodynamic factors and in the imines by a high kinetic barrier, caused by an incorrect orbital symmetry in the T_1 state. In the thiocarbonyl series, one solution would be to stabilize the 1,5-HAT product through additional substitution at the H atom donor site. In the imine series, the use of charged functional groups or Lewis acids could be used to reorder the nπ* and ππ* states, analogous to analogous to recent studies of this and related chemistry.[12, 55-58]

This study predicts a significantly expanded scope for the Diels-Alder reaction of photo-generated dienes than existing literature. The re-aromatization that occurs during the cycloaddition event appears to greatly enhance the reactivity of the *o*-QDM diene relative to a typical 1,3-butadiene. Moreover, this work shows that the presence of additional ring substituents are likely to further enhance this reactivity to such an extent that otherwise unreactive dienophiles such as ethylene should react rapidly at room temperature. Our calculations also question the commonly held view that TS asynchronicity and reactivity are inversely related.

Finally, we show that the enhanced reactivity of photo-generated *o*-QDMs should permit the first concerted and uncatalyzed (4+1)cycloadditions between dienes and CO. We predict that this unique sequence will provide access benzannelated cyclopentanones in short order. Efforts are underway to examine the synthetic feasibility, scope and applications of the process.

METHODS

Computational Procedures. Standard density functional theory (DFT) and time-dependent density functional theory (TD-DFT) calculations were performed using the Gaussian 16 electronic structure package.[70] The level of theory was chosen on the basis of our previous studies of PEDA reactions,[11, 12] and related photochemical processes.[55, 57, 58, 71] Where possible, calculated spectra were benchmarked against experiment, and also against those obtained using other levels of theory (vide infra). Unless noted otherwise, geometries were optimized at the M06-2X[72]/6-31+G(d,p) level of theory; TD-DFT calculations of excited states were performed at the same level of theory. Solvent corrections in dichloromethane and dimethyl sulfoxide were obtained with the SMD continuum solvent model.[73] For potential energy surfaces, the thermocycle approach was employed to determine the 298 K Gibbs free energies in solution in conjunction with the ideal gas partition functions under harmonic oscillator – rigid rotor aproximation.[74] All energies given are from the conformationally searched, global minimum energy structures in both gas and solvent phases, unless otherwise indicated. Stability analysis was employed to approximately locate conical intersection points, an approach that we have validated previously for PEDA reactions (see Appendix S7.23, Supporting Information).[12] Intrinsic reaction coordinate (IRC) calculations[75] were used to verify the nature and connectivity of key transition states. UV-Vis spectra were visualized within Gaussview[76] using default parameters. The orbital character of calculated photochemical transitions were manually assigned by projecting canonical orbitals into Natural Transition Orbitals (NTOs)[77] and inspecting the transition density matrix within Gaussview.

Experimental Procedures. 2-Tolualdehyde (**1**), 2-methylacetophenone (**2**), and 2-methylbenzophenone (**3**) were used as purchased without further purification. 1-(*o*-Tolyl)ethane-1-thione (**5**) and phenyl(*o*-tolyl)methanethione (**6**) were prepared from their corresponding ketones (i.e., **2** and **3**) using Lawesson's reagent[78] via the procedure based on that of Jaiswal and co-workers.[79] 4-Methyl-*N*-(2-methylbenzylidene)benzenesulfonamide[80] **7a** and 4-methyl-*N*-(1-(*o*-tolyl)ethylidene)benzenesulfonamide[81] **8a** were prepared from the corresponding ketones by literature procedures, the latter of which were also used to

prepare 4-methyl-*N*-(phenyl(o-tolyl)methylene)benzenesulfonamide **9a**.[81] UV/vis spectroscopy measurements were performed on an Agilent Technologies Cary 60 spectrometer in quartz cuvettes (path length = 1 cm). Background subtractions were performed at the beginning of each new day or when a different cuvette was used. For each compound, standard solutions in DMSO with concentrations in the range of 0.01-0.20 mM were prepared and Beers law calibration curves were established. For full experimental details including detailed synthetic procedures, compound characterisation data, and UV-vis spectroscopy, the reader is referred to the Supporting Information (Appendices S1-S3).

ASSOCIATED CONTENT

Supporting Information

PDF File containing full experimental details including synthetic procedures, characterization data, ^{1}H and ^{13}C NMR spectra, UV-vis spectra, and all computational data including Jablonski diagrams potential energy surfaces, TD-DFT results, total energies and geometries. The Supporting Information is available free of charge on the ACS Publications website.

Corresponding Author

* Email: michelle.coote@anu.edu.au

ACKNOWLEDGMENT

The authors thank Dr Ben Noble for many useful discussions and his assistance with preparing Scheme 3, and also gratefully acknowledge an ARC Laureate Fellowship (to M.L.C.), an ARC Discovery Grant (to MSS), and generous supercomputing time from the National Computational Infrastructure.

Funding Sources

Australian Research Council (FL170100041, DP160104322)

REFERENCES

1. Weedon, A. C., Photochemical reactions involving enols. In *Enols (1990)*, 1990; pp 591-638.
2. Lienhard, G. E.; Wang, T.-C., Mechanism of acid-catalyzed enolization of ketones. *J. Am. Chem. Soc.* **1969,** *91*, 1146-1153.
3. Toullec, J., Enolisation of Simple Carbonyl Compounds and Related Reactions. In *Advances in Physical Organic Chemistry*, Gold, V.; Bethell, D., Eds. Academic Press: 1982; Vol. 18, pp 1-77.
4. Klán, P.; Wirz, J.; Gudmundsdottir, A. D., Photoenolization and Its Applications In *CRC Handbook of Organic Photochemistry and Photobiology, Third Edition - Two Volume Set*, CRC Press: 2012.
5. Yang, N. C.; Rivas, C., A new photochemical primary process, the photochemical enolization of o-substituted benzophenones. *J. Am. Chem. Soc.* **1961,** *83*, 2213-2213.
6. Sammes, P. G., Photoenolisation. *Tetrahedron* **1976,** *32*, 405-422.
7. Haag, R.; Wirz, J.; Wagner, P. J., The Photoenolization of 2-Methylacetophenone and Related Compounds. *Helv. Chim. Acta* **1977,** *60*, 2595-2607.
8. Findlay, D. M.; Tchir, M. F., Photoenolization of ortho-alkyl-substituted acetophenones: evidence for the enol triplet state. *J. Chem. Soc. Faraday Trans. 1* **1976,** *72*, 1096-1100.
9. Lutz, H.; Bréhéret, E.; Lindqvist, L., Photoenolization of ortho-methyl-substituted acetophenones: solvent effects on the triplet state reactivity. *J. Chem. Soc. Faraday Trans. 1* **1973,** *69*, 2096-2102.
10. Migani, A.; Blancafort, L.; Robb, M. A.; DeBellis, A. D., An Extended Conical Intersection Seam Associated with a Manifold of Decay Paths: Excited-State Intramolecular Proton Transfer in O-Hydroxybenzaldehyde. *J. Am. Chem. Soc.* **2008,** *130*, 6932-6933.
11. Menzel, J. P.; Noble, B. B.; Lauer, A.; Coote, M. L.; Blinco, J. P.; Barner-Kowollik, C., Wavelength Dependence of Light-Induced Cycloadditions. *J. Am. Chem. Soc.* **2017,** *139*, 15812-15820.
12. Blyth, M. T.; Noble, B. B.; Russell, I. C.; Coote, M. L., Oriented Internal Electrostatic Fields Cooperatively Promote Ground- and Excited-State Reactivity: A Case Study in Photochemical CO2 Capture. *J. Am. Chem. Soc.* **2020,** *142*, 606-613.
13. Quinkert, G.; Schwartz, U.; Stark, H.; Weber, W.-D.; Baier, H.; Adam, F.; Dürner, G., Asymmetric Total Synthesis of (+)-Estrone. *Angew. Chem. Int. Ed.* **1980,** *19*, 1029-1030.
14. Quinkert, G.; Weber, W.-D.; Schwartz, U.; Dürner, G., A Photochemical Route to (7±)-Estrone. *Angew. Chem. Int. Ed.* **1980,** *19*, 1027-1029.
15. Prabhakar, S.; Lobo, A. M.; Oliveira, I. M. C., Photochemical approach to the rhoeadine alkaloid skeleton: synthesis of (±)-cis-alpinigenine. *J. Chem. Soc. Chem. Commun.* **1977**, 419-420.
16. Prabhakar, S.; Lobo, A. M.; Tavares, M. R.; Oliveira, I. M. C., Total synthesis of the alkaloids (±)-alpinigenine and (±)-cis-alpinigenine. *J. Chem. Soc Perkin Trans. 1* **1981**, 1273-1277.
17. Andrews, R. C.; Teague, S. J.; Meyers, A. I., Asymmetric total synthesis of (-)-podophyllotoxin. *J. Am. Chem. Soc.* **1988,** *110*, 7854-7858.
18. Kraus, G. A.; Wu, Y., Hydrogen atom abstraction reactions in organic synthesis. A formal total synthesis of racemic podophyllotoxin. *J. Org. Chem.* **1992,** *57*, 2922-2925.
19. Kraus, G. A.; Zhao, G., A Direct Synthesis of the Dimethyl Ether of Benzo[a]naphthacenequinone G-2N. *Synlett* **1995,** *1995*, 541-542.
20. Kraus, G. A.; Zhao, G., Direct Synthesis of G-2N. *J. Org. Chem.* **1996,** *61*, 2770-2773.
21. Kraus, G. A.; Chen, L., Photoenolization Reactions in Organic Synthesis. A Direct Synthesis of 4-Deoxyaklavinone. *Synlett* **1991,** *1991*, 51-52.
22. Kraus, G. A.; Chen, L., The Development of a Direct Synthetic Route to Pleurotin. *Synlett* **1991,** *1991*, 89-90.
23. Kraus, G. A.; Chen, L.; Jacobson, R. A., Synthesis and Evaluation of a Pleurotin Analog. *Synth. Commun.* **1993,** *23*, 2041-2049.
24. Nicolaou, K. C.; Gray, D. L. F., Total Synthesis of Hybocarpone and Analogues Thereof. A Facile Dimerization of Naphthazarins to Pentacyclic Systems. *J. Am. Chem. Soc.* **2004,** *126*, 607-612.
25. Trost, B. M.; Pissot-Soldermann, C.; Chen, I., A Short and Concise Asymmetric Synthesis of Hamigeran B. *Chem. Eur. J.* **2005,** *11*, 951-959.
26. Yang, B.; Lin, K.; Shi, Y.; Gao, S., Ti(Oi-Pr)4-promoted photoenolization Diels–Alder reaction to construct polycyclic rings and its synthetic applications. *Nat. Commun.* **2017,** *8*, 622.
27. Lu, X.-L.; Yang, B.; He, H.; Gao, S., Synthesis of polycyclic naphthols and naphthalenes via tandem Ti(Oi-Pr)4-promoted photoenolization Diels–Alder reaction and aromatization. *Org. Chem. Front.* **2021,** *8*, 1143-1148.
28. Xue, D.-s.; Xu, M.; Zheng, C.; Yang, B.; Hou, M.; He, H.; Gao, S., Titanium-promoted Intramolecular Photoenolization/Diels-Alder Reaction to Construct Polycyclic Terpenoids: Formal Synthesis of Mycoleptodiscin A. *Chinese J. Chem.* **2019,** *37*, 135-139.
29. Lu, X.-L.; Qiu, Y.; Yang, B.; He, H.; Gao, S., Asymmetric total synthesis of (+)-xestoquinone and (+)-adociaquinones A and B. *Chem. Sci.* **2021,** *12*, 4747-4752.
30. Fairbanks, B. D.; Macdougall, L. J.; Mavila, S.; Sinha, J.; Kirkpatrick, B. E.; Anseth, K. S.; Bowman, C. N., Photoclick Chemistry: A Bright Idea. *Chem. Rev.* **2021,** *121*, 6915-6990.

31. Pelliccioli, A. P.; Wirz, J., Photoremovable protecting groups: reaction mechanisms and applications. *Photochem. Photobiol. Sci.* **2002,** *1*, 441-458.

32. Griesbeck, A. G.; Porschen, B.; Kropf, C.; Landes, A.; Hinze, O.; Huchel, U.; Gerke, T., Photocaged Hydrocarbons, Aldehydes, Ketones, Enones, and Carboxylic Acids and Esters that Release by the Norrish II Cleavage Protocol and Beyond: Controlled Photoinduced Fragrance Release. *Synthesis* **2017,** *49*, 539-553.

33. Nicolaou, K. C.; Gray, D. L. F.; Tae, J., Total Synthesis of Hamigerans and Analogues Thereof. Photochemical Generation and Diels−Alder Trapping of Hydroxy-o-quinodimethanes. *J. Am. Chem. Soc.* **2004,** *126*, 613-627.

34. Yang, B.; Wen, G.; Zhang, Q.; Hou, M.; He, H.; Gao, S., Asymmetric Total Synthesis and Biosynthetic Implications of Perovskones, Hydrangenone, and Hydrangenone B. *J. Am. Chem. Soc.* **2021,** *143*, 6370-6375.

35. Kärkäs, M. D.; Porco, J. A.; Stephenson, C. R. J., Photochemical Approaches to Complex Chemotypes: Applications in Natural Product Synthesis. *Chem. Rev.* **2016,** *116*, 9683-9747.

36. Griesbeck, A. G.; Stadtmüller, S., ω-Hydroxy-ortho-quinodimethane: trapping with trifluoroacetone and photocyclization. *Chem. Ber.* **1993,** *126*, 2149-2150.

37. Hopkinson, M. N.; Mavroskoufis, A., Photo-NHC Catalysis: Accessing Ketone Photochemistry with Carboxylic Acid Derivatives. *Synlett* **2021,** *32*, 95-101.

38. Masuda, Y.; Ishida, N.; Murakami, M., Light-Driven Carboxylation of o-Alkylphenyl Ketones with CO2. *J. Am. Chem. Soc.* **2015,** *137*, 14063-14066.

39. Hu, Y.; Pan, D.; Cong, L.; Yao, Y.; Yu, C.; Li, T.; Yao, C., NHC-Catalyzed Efficient Syntheses of Isoquinolinones or Isochromanones through Formal [4+2] Cycloaddition of o-Quinodimethanes with Acylhydrazones or Ketones. *ChemistrySelect* **2018,** *3*, 1708-1712.

40. Kuznetsov, D. M.; Kutateladze, A. G., Step-Economical Photoassisted Diversity-Oriented Synthesis: Sustaining Cascade Photoreactions in Oxalyl Anilides to Access Complex Polyheterocyclic Molecular Architectures. *J. Am. Chem. Soc.* **2017,** *139*, 16584-16590.

41. Kuznetsov, D. M.; Mukhina, O. A.; Kutateladze, A. G., Photoassisted Synthesis of Complex Molecular Architectures: Dearomatization of Benzenoid Arenes with Aza-o-xylylenes via an Unprecedented [2+4] Reaction Topology. *Angew. Chem. Int. Ed.* **2016,** *55*, 6988-6991.

42. Mukhina, O. A.; Kutateladze, A. G., Oxazolines as Dual-Function Traceless Chromophores and Chiral Auxiliaries: Enantioselective Photoassisted Synthesis of Polyheterocyclic Ketones. *J. Am. Chem. Soc.* **2016,** *138*, 2110-2113.

43. Mukhina, O. A.; Kuznetsov, D. M.; Cowger, T. M.; Kutateladze, A. G., Amino Azaxylylenes Photogenerated from o-Amido Imines: Photoassisted Access to Complex Spiro-Poly-Heterocycles. *Angew. Chem. Int. Ed.* **2015,** *54*, 11516-11520.

44. Das, A.; Thomas, S. S.; Garofoli, A. A.; Chavez, K. A.; Krause, J. A.; Bohne, C.; Gudmundsdottir, A. D., Steric Demand and Rate-determining Step for Photoenolization of Di-ortho-substituted Acetophenone Derivatives. *Photochem. Photobiol.* **2019,** *95*, 154-162.

45. El-Sayed, M. A., Triplet state. Its radiative and nonradiative properties. *Acc. Chem. Res.* **1968,** *1*, 8-16.

46. Ziółek, M.; Kubicki, J.; Maciejewski, A.; Naskręcki, R.; Grabowska, A., Enol-keto tautomerism of aromatic photochromic Schiff base N,N′-bis(salicylidene)-p-phenylenediamine: Ground state equilibrium and excited state deactivation studied by solvatochromic measurements on ultrafast time scale. *J. Chem. Phys.* **2006,** *124*, 124518.

47. Padwa, A., Photochemistry of the carbon-nitrogen double bond. *Chem. Rev.* **1977,** *77*, 37-68.

48. Pratt, A. C., The photochemistry of imines. *Chem. Soc. Rev.* **1977,** *6*, 63-81.

49. Gao, F.; Ye, X.; Li, H.; Zhong, X.; Wang, Q., Evidence for Two-Photon Absorption-Induced ESIPT of Chromophores Containing Hydroxyl and Imino Groups. *Chemphyschem* **2012,** *13*, 1313-1324.

50. Massaro, R. D.; Blaisten-Barojas, E., Theoretical investigation of the photophysics of methyl salicylate isomers. *J. Chem. Phys.* **2011,** *135*, 164306.

51. Li, C.-X.; Guo, W.-W.; Xie, B.-B.; Cui, G., Photodynamics of oxybenzone sunscreen: Nonadiabatic dynamics simulations. *J. Chem. Phys.* **2016,** *145*, 074308.

52. Lochbrunner, S.; Schultz, T.; Schmitt, M.; Shaffer, J. P.; Zgierski, M. Z.; Stolow, A., Dynamics of excited-state proton transfer systems via time-resolved photoelectron spectroscopy. *J. Chem. Phys.* **2001,** *114*, 2519-2522.

53. L. Sobolewski, A.; Domcke, W., Abinitio potential-energy functions for excited state intramolecular proton transfer: a comparative study of o-hydroxybenzaldehyde, salicylic acid and 7-hydroxy-1-indanone. *Phys. Chem. Chem. Phys.* **1999,** *1*, 3065-3072.

54. Kandappa, S. K.; Valloli, L. K.; Ahuja, S.; Parthiban, J.; Sivaguru, J., Taming the excited state reactivity of imines – from non-radiative decay to aza Paternò–Büchi reaction. *Chem. Soc. Rev.* **2021,** *50*, 1617-1641.

55. Marlton, S. J. P.; McKinnon, B. I.; Hill, N. S.; Coote, M. L.; Trevitt, A. J., Electrostatically Tuning the Photodissociation of the Irgacure 2959 Photoinitiator in the Gas Phase by Cation Binding. *J. Am. Chem. Soc.* **2021,** *143*, 2331-2339.

56. Hill, N. S.; Coote, M. L., Strategies for Red-Shifting Type I Photoinitiators: Internal Electric Fields versus Lewis Acids versus Increasing Conjugation. *Aust. J. Chem.* **2019,** *72*, 627-632.

57. Hill, N. S.; Coote, M. L., Internal Oriented Electric Fields as a Strategy for Selectively Modifying Photochemical Reactivity. *J. Am. Chem. Soc.* **2018,** *140*, 17800-17804.

58. Noble, B. B.; Mater, A. C.; Smith, L. M.; Coote, M. L., The effects of Lewis acid complexation on type I radical photoinitiators and implications for pulsed laser polymerization. *Polym. Chem.* **2016,** *7*, 6400-6412.

59. Degirmenci, I.; Coote, M. L., Comparison of Thiyl, Alkoxyl, and Alkyl Radical Addition to Double Bonds: The Unusual Contrasting Behavior of Sulfur and Oxygen Radical Chemistry. *J. Phys. Chem. A* **2016,** *120*, 1750-1755.

60. Degirmenci, I.; Coote, M. L., Effect of Substituents on the Stability of Sulfur-Centered Radicals. *J. Phys. Chem. A* **2016,** *120*, 7398-7403.

61. For a previously reported indanone synthesis, which was presumed to involve an oxidative insertion mechanism, see: Bonfantini, E.; Métral, J.-L.; Vogel, P., Ironcarbonyl Complexes of 5,6-Dimethylidene-7-oxabicyclo[2.2.1]hept-2-ene Derivatives. Synthesis of Substituted Tricarbonyl(ortho-quinodimethane)iron Complexes and 2-Indanones. *Helv. Chim. Acta* **1987**, *70*, 1791-1797.

62. Zhou, Y.-Y.; Uyeda, C., Catalytic reductive [4 + 1]-cycloadditions of vinylidenes and dienes. *Science* **2019,** *363*, 857-862.

63. Trost, B. M.; Abell, A. D.; Bauer, I.; Daly, E. M.; Diène, C. R.; Diver, S. T.; Edmonds, M. K.; Gandon, V.; Grainger, R. S.; Jervis, P. J., et al., Synthesis by Extrusion. In *Category 6, Compounds with All-Carbon Functions*, 1st Edition ed.; Georg Thieme Verlag: Stuttgart, 2009; Vol. 46.

64. Rickborn, B., The Retro–Diels–Alder Reaction Part I. C=C Dienophiles. *Org. React.* **1998,** *52*, 1-393.

65. Monnat, F.; Vogel, P.; Meana, R.; Sordo, J. A., Equilibrium and Kinetic Deuterium Isotope Effects on the Hetero-Diels–Alder Addition of Sulfur Dioxide. *Angew. Chem. Int. Ed.* **2003,** *42*, 3924-3927.

66. Sauer, J., Diels-Alder reactions II: The Reaction Mechanism. *Angew. Chem. Int. Ed.* **1967,** *6*, 16-33.

67. Lording, W. J.; Fallon, T.; Sherburn, M. S.; Paddon-Row, M. N., The simplest Diels–Alder reactions are not endo-selective. *Chem. Sci.* **2020,** *11*, 11915-11926.

68. Houk, K. N.; Liu, F.; Yang, Z.; Seeman, J. I., Evolution of the Diels–Alder Reaction Mechanism since the 1930s: Woodward, Houk with Woodward, and the Influence of Computational Chemistry on Understanding Cycloadditions. *Angew. Chem. Int. Ed.* **2021,** *60*, 12660-12681.

69. Vermeeren, P.; Tiezza, M. D.; van Dongen, M.; Fernández, I.; Bickelhaupt, F. M.; Hamlin, T. A., Lewis Acid-Catalyzed Diels-Alder Reactions: Reactivity Trends across the Periodic Table. *Chem. Eur. J.* **2021,** *27*, 10610-10620.

70. Frisch, M. J.; Trucks, G. W.; Schlegel, H. B.; Scuseria, G. E.; Robb, M. A.; Cheeseman, J. R.; Scalmani, G.; Barone, V.; Petersson, G. A.; Nakatsuji, H., et al., *Gaussian 09, Revision E.01*. Gaussian, Inc.: Wallingford CT, 2016.

71. Hill, N. S.; Fule, M. J.; Morris, J.; Clément, J.-L.; Guillaneuf, Y.; Gigmes, D.; Coote, M. L., Mesolytic Versus Homolytic Cleavage in Photochemical Nitroxide-Mediated Polymerization. *Macromolecules* **2020,** *53*, 1567-1572.

72. Zhao, Y.; Truhlar, D. G., The M06 suite of density functionals for main group thermochemistry, thermochemical kinetics, noncovalent interactions, excited states, and transition elements: two new functionals and systematic testing of four M06-class functionals and 12 other functionals. *Theor. Chem. Acc.* **2008,** *120*, 215-241.

73. Marenich, A. V.; Cramer, C. J.; Truhlar, D. G., Universal Solvation Model Based on Solute Electron Density and on a Continuum Model of the Solvent Defined by the Bulk Dielectric Constant and Atomic Surface Tensions. *J. Phys. Chem. B* **2009,** *113*, 6378-6396.

74. Ho, J. M.; Klamt, A.; Coote, M. L., Comment on the Correct Use of Continuum Solvent Models. *J. Phys. Chem. A* **2010,** *114*, 13442-13444.

75. Hratchian, H. P.; Schlegel, H. B., Finding Minima, Transition States, and Following Reaction Pathways on Ab Initio Potential Energy Surfaces. In *Theory and Applications of Computational Chemistry: The First 40 Years*, Dykstra, C. E.; Frenking, G.; Kim, K. S.; Scuseria, G., Eds. Elsevier: Amsterdam, 2005; pp 195-249.

76. Dennington, R.; Keith, T. A.; Millam, J. M., *GaussView, Version 6*. Semichem, Inc.: Shawnee Mission KS, 2016.

77. Martin, R. L., Natural transition orbitals. *J. Chem. Phys.* **2003,** *118*, 4775-4777.

78. Ozturk, T.; Ertas, E.; Mert, O., Use of Lawesson's Reagent in Organic Syntheses. *Chem. Rev.* **2007,** *107*, 5210-5278.

79. Jaiswal, V.; Mondal, B.; Singh, K.; Das, D.; Saha, J., [3 + 2]-Annulation of Azaoxyallyl Cations and Thiocarbonyls for the Assembly of Thiazolidin-4-ones. *Org. Lett.* **2019,** *21*, 5848-5852.

80. Ueno, S.; Ohtsubo, M.; Kuwano, R., [4+2] Cycloaddition of o-Xylylenes with Imines Using Palladium Catalyst. *J. Am. Chem. Soc.* **2009,** *131*, 12904-12905.

81. Ortiz, P.; Collados, J. F.; Harutyunyan, S. R., Direct Synthesis of Enolizable N-Sulfonyl Ketimines Under Microwave Irradiation. *Eur. J. Org. Chem.* **2016,** *2016*, 1247-1250.

Table of Contents artwork